

1 **Large amplitude electrostatic proton plasma frequency**  
2 **waves in the magnetospheric separatrix and outflow**  
3 **regions during magnetic reconnection**

4 **K. Steinvall<sup>1,2</sup>, Yu. V. Khotyaintsev<sup>1</sup>, D. B. Graham<sup>1</sup>, A. Vaivads<sup>3</sup>, M.**  
5 **André<sup>1</sup>, C. T. Russell<sup>4</sup>**

6 <sup>1</sup>Swedish Institute of Space Physics, Uppsala, Sweden

7 <sup>2</sup>Space and Plasma Physics, Department of Physics and Astronomy, Uppsala University, Uppsala, Sweden

8 <sup>3</sup>Division of Space and Plasma Physics, School of Electrical Engineering and Computer Science, KTH

9 Royal Institute of Technology, Stockholm, Sweden

10 <sup>4</sup>Institute of Geophysics and Planetary Physics, University of California, Los Angeles, CA, USA

11 **Key Points:**

- 12 • Large amplitude electrostatic waves are found in the magnetospheric separatrix  
13 region
- 14 • The waves are driven by an ion acoustic instability due to the presence of cold ions
- 15 • The ion acoustic waves may heat cold magnetospheric ions and dissipate paral-  
16 lel currents

---

Corresponding author: Konrad Steinvall, [konrad.steinvall@irfu.se](mailto:konrad.steinvall@irfu.se)

## 17 **Abstract**

18 We report Magnetospheric Multiscale observations of large amplitude, parallel, electro-  
 19 static, proton plasma frequency waves on the magnetospheric side of the reconnecting  
 20 magnetopause. The waves are often found in the magnetospheric separatrix region and  
 21 in the outflow close to the magnetospheric ion edge. Statistical results from five months  
 22 of data show that these waves are closely tied to the presence of cold (typically tens of  
 23 eV) ions, found for 91% of waves in the separatrix region, and that plasma properties  
 24 are consistent with ion acoustic wavegrowth. We analyze one wave event in detail, con-  
 25 cluding that the wave is ion acoustic. We provide a simple explanation for the mecha-  
 26 nisms leading to the development of the ion acoustic instability. These waves can be im-  
 27 portant for separatrix dynamics, by heating the cold ion component and providing a mech-  
 28 anism to damp the kinetic Alfvén waves propagating away from the reconnection site.

## 29 **Plain Language Summary**

30 The magnetopause is the magnetic boundary shielding the Earth’s magnetosphere  
 31 from the shocked solar wind plasma of the magnetosheath. Magnetic reconnection, a fun-  
 32 damental plasma process, locally breaks this boundary, leading to energization and mix-  
 33 ing of magnetospheric and solar wind plasma. During the reconnection process, the plasma  
 34 is highly unstable and many different kinds of waves appear. In this Letter we investi-  
 35 gate the large amplitude electrostatic waves with frequencies around the proton plasma  
 36 frequency which are often found in spacecraft observations of magnetic reconnection. We  
 37 find that the waves can appear when cold (tens of eV) magnetospheric ions are present  
 38 at the magnetopause, and are generated by an ion acoustic instability between the cold  
 39 ions and the fast flowing electrons often observed during magnetic reconnection. The waves  
 40 might heat the cold ions and couple to the large scales by dissipating parallel currents.

## 41 **1 Introduction**

42 The magnetopause is the boundary between the Earth’s magnetosphere and the  
 43 shocked solar wind plasma of the magnetosheath. Plasma waves are often found in the  
 44 vicinity of the magnetopause (e.g. Fairfield, 1976; Gurnett et al., 1979; LaBelle et al.,  
 45 1987; Tang et al., 2019), and appear to be intimately connected to magnetic reconnect-  
 46 tion (Khotyaintsev et al., 2019), a fundamental plasma process where changes in mag-  
 47 netic field topology result in plasma mixing and explosive energy conversion from mag-

48 netic energy to kinetic and thermal energy (e.g. Birn & Priest, 2007). Though magnetic  
49 reconnection is a well studied subject some fundamental aspects are still not understood,  
50 and studying wave dynamics might be crucial to fully understand the cause and effects  
51 of magnetic reconnection (Khotyaintsev et al., 2019; Wilder et al., 2019).

52 The separatrix region is defined as the kinetic boundary separating the inflow and  
53 outflow regions of magnetic reconnection (Lindstedt et al., 2009). As such, this region  
54 is characterized by recently reconnected magnetic field lines, complex distribution func-  
55 tions, and large parallel currents (Khotyaintsev et al., 2006). At the reconnecting day-  
56 side magnetopause, which is the focus of this Letter, the complexity is even greater due  
57 to the variable plasma composition, where the typically tenuous magnetosphere, which  
58 can contain both hot ( $\sim 1$  keV) and cold ( $\sim 10$  eV) plasma (André & Cully, 2012; Lee  
59 & Angelopoulos, 2014), is mixing with the dense  $\sim 100$  eV magnetosheath plasma. The  
60 end result is that the plasma is unstable to the generation of various waves, which are  
61 observed both in simulations and spacecraft data. Examples include beam and loss cone  
62 driven whistler waves (Graham, Vaivads, et al., 2016; Uchino et al., 2017), electron holes (Farrell  
63 et al., 2002; Graham et al., 2015), Langmuir waves (Vaivads et al., 2004; Wilder et al.,  
64 2016; Zhou et al., 2016), ion acoustic waves (Uchino et al., 2017), and electron acous-  
65 tic waves (Ergun, Holmes, et al., 2016).

66 Early observations from the Magnetospheric Multiscale (MMS) mission (Burch et  
67 al., 2016) reported the presence of electrostatic waves with large amplitude parallel (to  
68 the magnetic field) electric fields ( $E_{\parallel}$ ) in the magnetospheric separatrix region close to  
69 the electron diffusion region (Ergun, Holmes, et al., 2016). The waves could be found  
70 with frequencies both below and significantly above the ion plasma frequency  $f_{pi}$ . By  
71 comparing observations with simulations, the high frequency waves were argued to be  
72 consistent with electron acoustic waves driven by the interaction of a cold magnetospheric  
73 electron beam with a warmer electron beam of magnetosheath origin, while the mech-  
74 anism behind the lower frequency waves observed in the MMS data could not be deter-  
75 mined unambiguously. Uchino et al. (2017) used Time History of Events and Macroscale  
76 Interactions during Substorms (THEMIS) (Angelopoulos, 2008) data to investigate waves  
77 found in the innermost open boundary layer during dayside magnetopause reconnection.  
78 The authors presented one wave event similar to the low frequency waves found by Ergun,  
79 Holmes, et al. (2016) and concluded that the wave was generated by an ion acoustic in-

80 stability. However, to the best of our knowledge, no statistical study of these low frequency  
 81 waves has yet been published.

82 In this Letter we use data from MMS to study the large amplitude, electrostatic,  
 83 ion plasma frequency waves observed in and around the magnetospheric separatrix re-  
 84 gion during ongoing magnetic reconnection, looking to answer the questions: What is  
 85 the instability generating these waves? What effect do these wave have on the separa-  
 86 trix plasma dynamics? We present and analyze one wave event in Section 2 where we  
 87 use wave properties and dispersion analysis to conclude that the wave is driven by an  
 88 ion acoustic instability between cold magnetospheric ions and electrons carrying the strong  
 89 parallel currents often found in the separatrix region (Khotyaintsev et al., 2006), likely  
 90 associated with kinetic Alfvén waves propagating away from the reconnection site (Dai  
 91 et al., 2017; Dai, 2018; Huang et al., 2018). The wave amplitude is large enough to trap  
 92 parts of the cold ion distribution, and the instability implies the dissipation of parallel  
 93 currents. We then investigate the waves from a statistical perspective in Section 3 and  
 94 find that the waves have properties and are found in plasmas which are qualitatively con-  
 95 sistent with ion acoustic wavegrowth. These ion acoustic waves can be important for sep-  
 96 aratrix dynamics by providing a mechanism to dissipate the strong parallel currents present  
 97 there, thereby coupling Debye scale wave activity to large scale plasma dynamics.

## 98 **2 Wave observation example**

99 In this section we start by discussing large amplitude waves observed by MMS dur-  
 100 ing a crossing of the reconnecting magnetopause on the 24th of October 2015. The waves  
 101 are similar to the ones reported by Ergun, Holmes, et al. (2016) in that they are elec-  
 102 trostatic, have large  $E_{\parallel}$ , nonlinear waveforms, and frequencies close to  $f_{pi}$ . We then an-  
 103 alyze one wave in detail, placing it in the context of magnetic reconnection, and deter-  
 104 mine its generation mechanism and effect on the plasma dynamics.

105 We present an overview of this magnetopause crossing in Fig. 1. This event has pre-  
 106 viously been analyzed in the context of reconnection in the presence of cold ions by Toledo-  
 107 Redondo et al. (2017). Initially, MMS is located in the magnetosphere. At around 07:03:48  
 108 UT, highlighted by the red shaded area, MMS crosses the electron edge (Gosling et al.,  
 109 1990; Lindstedt et al., 2009) as seen by the sudden appearance of low energy magnetosheath  
 110 electrons and reduction of high energy magnetospheric electrons (Fig. 1b). Shortly af-

111 ter, around 07:03:51, MMS crosses the ion edge (green shaded region) where the first ions  
 112 of magnetosheath origin are observed (Fig. 1c) and enters the outflow region while re-  
 113 remaining close to the ion edge. During this time, strong parallel currents are observed  $j_{\parallel} \approx$   
 114  $500 \text{ nA/m}^2$  (Fig. 1f), together with waves (Fig. 1g) with amplitudes reaching up to 200  
 115 mV/m. There are no corresponding magnetic field fluctuations (not shown), meaning  
 116 the waves are electrostatic. The frequencies of the waves are slightly below the ion plasma  
 117 frequency  $f_{pi}$  (Fig. 1h), which indicates that ion dynamics are likely to play a role in  
 118 the generation mechanism.

119 In order to investigate the generation mechanism and understand how these waves  
 120 interact with the plasma, we zoom in to the large amplitude waves marked by the dashed  
 121 vertical line in Fig. 1, and plot the 1 and 2-dimensional velocity distribution functions  
 122 (VDFs) for ions (Figs. 2a,f-h) and electrons (Figs. 2b,i-k). The VDFs have been inte-  
 123 grated over the entire velocity range of FPI. In the case of ions, two components are clearly  
 124 visible. The cold component with  $v_{\parallel} \approx -20 \text{ km/s}$  corresponds to the cold magnetospheric  
 125 ions seen in Fig. 1c whereas the hotter component with  $v_{\parallel} \approx -500 \text{ km/s}$  and the char-  
 126 acteristic D-shape in Fig. 2f corresponds to transmitted magnetosheath ions moving along  
 127 reconnected field lines south of the x-line (Cowley, 2013), consistent with the southward  
 128 ion outflow in Fig. 1e. The gradual disappearance of low speed magnetosheath ions start-  
 129 ing after  $\sim 05:04:01$  in Fig. 2a indicates that the spacecraft is moving closer to the mag-  
 130 netospheric ion edge. The electron VDF primarily contains magnetosheath electrons, and  
 131 is slightly shifted in the  $-v_{\parallel}$  direction, corresponding to the positive  $j_{\parallel}$  in Fig. 1f. The  
 132 different plasma components and their distinct parallel bulk velocities constitute a sys-  
 133 tem where there are several positive slopes in the VDFs, and Landau resonance could  
 134 lead to spontaneous growth of different waves.

135 Before moving on to dispersion analysis, we briefly discuss the electrostatic prop-  
 136 erties of the wave shown in Figs. 2c-e. In particular we want to determine the wave's phase  
 137 velocity  $\mathbf{v}_{\phi} = v_{\phi} \hat{\mathbf{k}}$  for two reasons. The first reason is that  $v_{\phi}$  depends on the genera-  
 138 tion mechanism, and thus serves as a diagnostic to determine what instability generated  
 139 the wave. The second reason is that once  $v_{\phi}$  is known, the electrostatic potential can be  
 140 calculated as  $\Phi = \int \delta E v_{\phi} dt$ . In this case we are particularly interested in  $\Phi$  since the  
 141 waveform of  $\delta E$  is non-linear, raising two questions which require  $\Phi$  to answer: Is there  
 142 a net potential change  $\Delta\Phi$  associated with the waves? Is the non-linear waveform due  
 143 to electron or ion trapping? Since the wave is electrostatic,  $\mathbf{k} \times \delta\mathbf{E} = 0$ , and we can

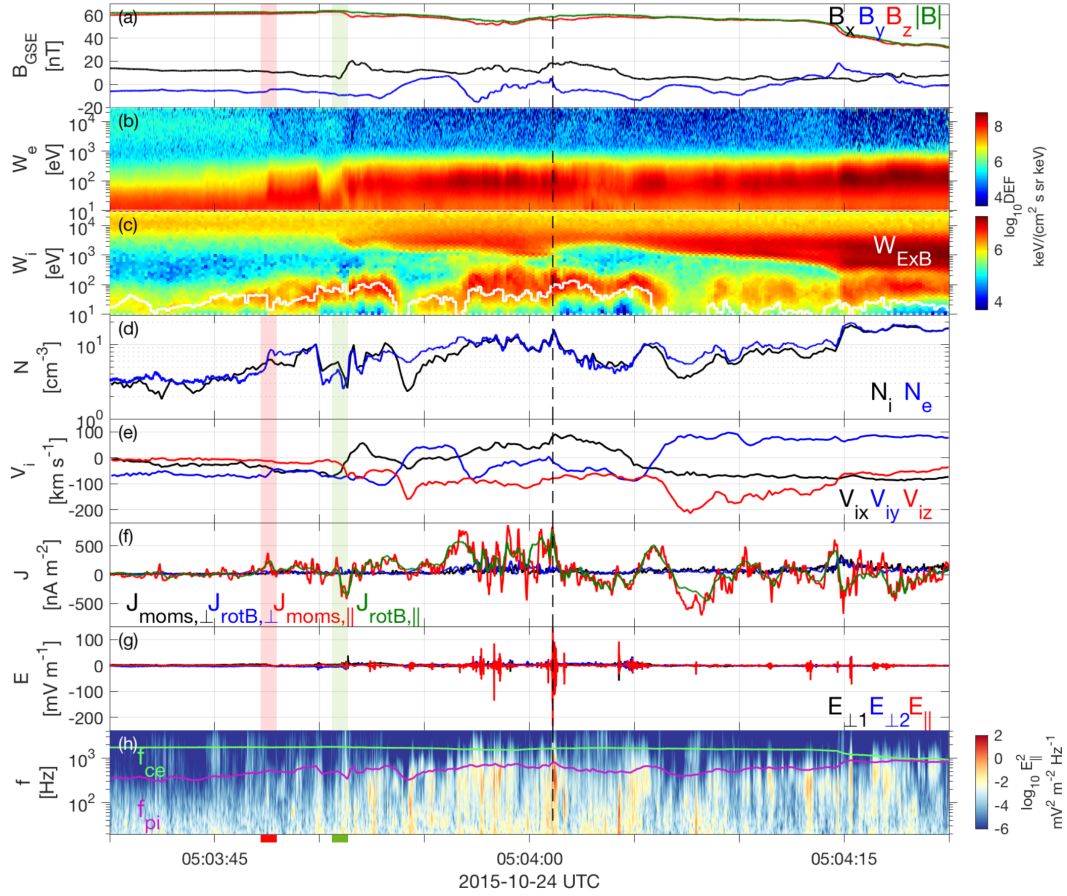


**Figure 1.** Overview of wave observation from MMS3. (a) Magnetic field data from the Fluxgate magnetometer (Russell et al., 2016) in the geocentric solar ecliptic (GSE) coordinate system. (b,c) Differential energy flux (DEF) from Fast Plasma Investigation (FPI) (Pollock et al., 2016) for electrons and ions. The white line in the ion spectrum is the energy corresponding to the  $\mathbf{E} \times \mathbf{B}$  drift. (d) Ion and electron density from FPI. The observed deviation from quasi-neutrality is artificial, mainly due to cold ions with energies below FPI's energy threshold. (e) Ion velocity from FPI in GSE. (f) Currents in magnetic field aligned coordinates calculated using  $\nabla \times \mathbf{B}$  and FPI plasma moments. (g) Electric field from the Electric field Double Probes (EDP) (Lindqvist et al., 2016; Ergun, Tucker, et al., 2016) in field aligned coordinates. (h) Spectral power density of  $E_{\parallel}$  where the green and purple lines correspond to the electron cyclotron and the ion plasma frequencies, respectively. The vertical red and green bars show roughly the location of the electron and ion edges.

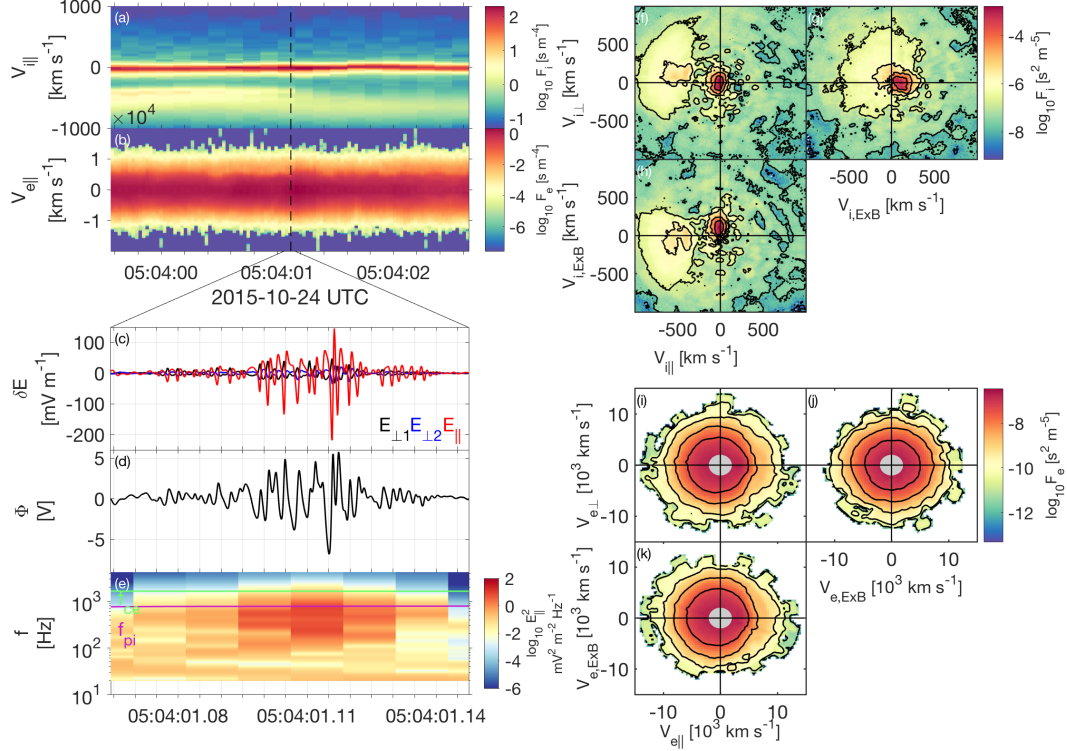


**Figure 2.** Particle distribution functions and wave properties observed by MMS3. (a,b) 1-dimensional ion and electron velocity distribution functions (VDFs). (c) Waveform of  $\mathbf{E}$  high-pass filtered at 100 Hz. (d) Electrostatic potential of the wave. (e) Spectral power density of  $E_{\parallel}$ . (f-h) 2-dimensional VDFs of ions sampled at 05:04:01.078. (i-k) 2-dimensional VDFs of electrons sampled at 05:04:01.108, marked by the vertical dashed line in panels (a) and (b). The central area of the 2-dimensional electron VDFs corresponding to energies not resolved by FPI are blocked out.

144 determine  $\hat{\mathbf{k}}$  using maximum variance analysis of  $\delta\mathbf{E}$ . We find that  $\pm\hat{\mathbf{k}}$  is field aligned  
 145 within the uncertainty. We determine  $v_\phi$  and the sign of  $\hat{\mathbf{k}}$  using cross-spectral analy-  
 146 sis of the electric field between the axial EDP probes (Graham, Khotyaintsev, et al., 2016)  
 147 and obtain  $v_\phi \approx -100$  km/s. We emphasize that this speed estimate has a large un-  
 148 certainty and should be interpreted only as a rough estimate. The sign, implying anti-  
 149 parallel propagation, is determined with much greater confidence. The slow  $v_\phi$  indicates  
 150 that the instability generating this wave is most likely an interaction between either the  
 151 two ion components, or the cold ions and the electrons. We calculate and plot  $\Phi$  in Fig. 2d.  
 152 Note that when calculating  $\Phi$ ,  $\delta E_\parallel$  is high-pass filtered at 100 Hz while  $\Phi$  is unfiltered,  
 153 and any  $\Delta\Phi$  related to the waves would appear in Fig. 2d. We conclude that there is no  
 154 significant potential change across the waves,  $\Delta\Phi = 0$ , and that the peak value of around  
 155  $\Phi = 5$  V corresponds to an ion trapping range  $v_{tr,i} = v_\phi \pm \sqrt{2e\Phi/m_i}$  of around  $(-130, -70)$   
 156 km/s, and equivalently an electron trapping range of around  $(-1100, 900)$  km/s in the  
 157 spacecraft frame. The waves are thus capable of trapping parts of both the cold ion and  
 158 electron components, which for example might lead to heating of the cold ions and lo-  
 159 cal flattening of the electron VDF.

160 We are now in a position to set up and solve the one-dimensional electrostatic dis-  
 161 persion relation (Fried & Conte, 1961)

$$162 \quad D(\omega, k) = 0 = 1 + \chi_{i,\text{cold}} + \chi_{i,\text{beam}} + \chi_{i,\text{bg}} + \chi_e, \quad (1)$$

163 where  $\chi_s(\omega, k)$  is the susceptibility of plasma component  $s$ . In addition to the plasma  
 164 components we discussed previously, we include a hot background ion component  $\chi_{i,\text{bg}}$ ,  
 165 corresponding to the hot magnetospheric ions in Fig. 1c. In Fig. 3a we show the observed  
 166 reduced 1-dimensional VDFs for ions and electrons as the gray circles and dots respec-  
 167 tively, and the Maxwellian fits by the solid lines. For the fits, we used the densities (units  
 168 of  $\text{cm}^{-3}$ )  $n_{i,\text{cold}} = 11.076$ ,  $n_{i,\text{beam}} = 0.48$ ,  $n_{i,\text{bg}} = 0.08$ ,  $n_e = 11.636$ , thermal speeds  
 169 (in km/s):  $v_{th;i,\text{beam}} = 180$ ,  $v_{th;i,\text{cold}} = 35$ ,  $v_{th;i,\text{bg}} = 900$ ,  $v_{th;e} = 4160$ , and parallel  
 170 drift speeds (in km/s):  $v_{d;i,\text{cold}} = 20$ ,  $v_{d;i,\text{beam}} = -580$ ,  $v_{d;i,\text{bg}} = -330$ ,  $v_{d;e} = -410$ .  
 171 The corresponding temperature ratio between the cold ions and the electrons is  $T_{i,\text{cold}}/T_e \approx$   
 172 0.13. Solving Eq. (1) numerically we find positive wavegrowth for the solution in Fig.  
 173 3b. The black(red) line corresponds to the real(imaginary) frequency  $\omega(\gamma)$ , and the cir-  
 174 cles mark the point of largest  $\gamma$ . The negative  $\omega$  implies propagating in the anti-parallel  
 175 direction, as was found in observations, and the phase speed at maximum growth marked  
 176 by the dashed line in Fig. 3a is  $v_{\text{max}(\gamma)} = -102$  km/s, close to the observed  $v_\phi$ .  $v_{\text{max}(\gamma)}$

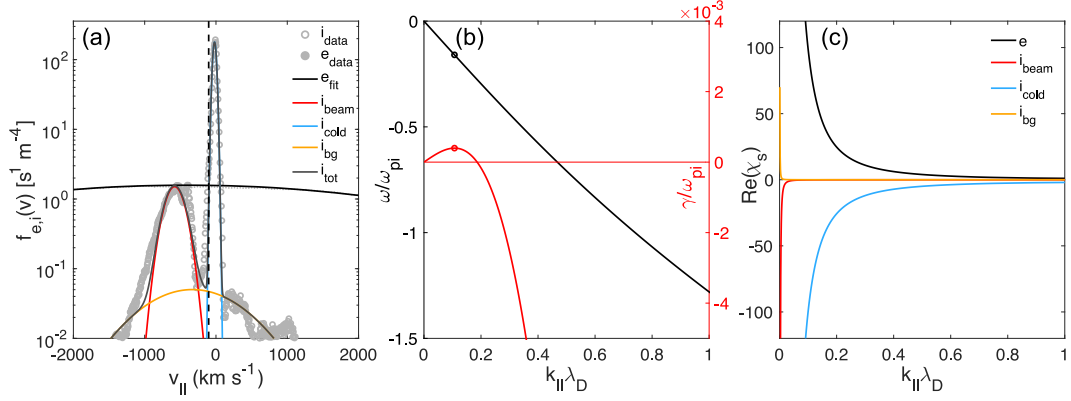


**Figure 3.** Dispersion analysis. (a) Observed and fitted reduced VDFs. The dashed line corresponds to the phase speed of the fastest growing wave. (b) Dispersion relation. The circles mark the points corresponding to the highest growth rate, and  $\lambda_D$  is the Debye length. (c) Real part of the susceptibilities of the plasma components for the solution in (b).

177 coincides with a positive slope of the drifting electron VDF, thus driving the wave via  
 178 Landau resonance. In Fig. 3c, we plot the real part of the different  $\chi_s$  and confirm that  
 179 the wave is due to the electrons and cold ions. The imaginary parts of  $\chi_s$  (not shown)  
 180 show similar results. The ion-ion instability is stabilized by the electrons in this case.  
 181 We thus conclude that an ion acoustic instability is the source behind the observed waves.

182  
 183 In summary, for this event we find  $E_{\parallel}$  waves with frequency close to  $f_{pi}$  in the re-  
 184 connection outflow, near the magnetospheric ion edge. The analyzed wave is propagat-  
 185 ing slowly ( $v_{\phi} \approx 100$  km/s) in the anti-parallel direction, carries no  $\Delta\Phi$ , and can trap  
 186 parts of the electron and cold ion distributions. Dispersion analysis shows that the plasma  
 187 is unstable to an ion acoustic instability between the dominating cold ions and the drift-  
 188 ing electrons.

### 189 3 Statistics

190 Armed with the knowledge from the previous section, we would like to see if the  
 191 ion acoustic instability can explain the wave observations also on a statistical level. To  
 192 investigate this, we scan through 5 months of MMS data when the four spacecraft are  
 193 close to the dayside magnetopause (September through November 2015, and October through  
 194 November 2016), searching for magnetopause crossings where waves with  $E_{\parallel} > 20$  mV/m

195 and maximum power within the frequency band  $[0.5, 2]f_{pi}$  are observed on the magne-  
 196 toshpheric side. We find that when the waves are observed in the separatrix region be-  
 197 tween the ion and electron edges, cold ions are present for 91% (233/255) of the events.  
 198 The waves where no cold ions are present tend to be either solitary waves or have a very  
 199 small number of wave periods, and we exclude these from the following analysis. The  
 200 wavevectors are typically close to field aligned, and the median wave normal angle is  $16^\circ$ .  
 201 We are unfortunately not able to determine  $v_\phi$  on a statistical level. This is primarily  
 202 because  $B_z$  is generally the dominant magnetic field component, and the axial EDP probes  
 203 are not ideal for interferometry due to their short separation and floating potential dif-  
 204 ference compared to the spin-plane probes used to calculate the spacecraft potential (Graham  
 205 et al., 2015). However, when we are able to roughly estimate  $v_\phi$  using either the spin-  
 206 plane or axial probes, we typically find  $v_\phi$  to be small  $\sim 100$  km/s, similar to the ex-  
 207 ample in Fig. 2. Since cold ions are present during most wave observations they are most  
 208 likely essential for the generation mechanism, motivating a statistical investigation into  
 209 the plasma composition. In order to easily compute the moments of the cold ion com-  
 210 ponent we take the wave events where the energy,  $W_{E \times B}$ , corresponding to the  $\mathbf{E} \times \mathbf{B}$   
 211 drift is close to the differential energy flux peak of the cold ions. We then compute the  
 212 cold ion moments by integrating the distribution function from the lowest energy to roughly  
 213  $2.1W_{E \times B}$  to ensure that we capture the whole cold ion distribution and ignore any hot  
 214 plasma. We only do this calculation when there is a clear energy separation between dif-  
 215 ferent ion components, resulting in 95 events gathered from 21 different orbits. In Fig. 4a  
 216 we present the results. There is a clear trend that these waves are primarily found when  
 217 the cold ions dominate  $n_{i,cold}/n_i \gtrsim 0.6$ , the cold ion temperature is much smaller than  
 218 the electron temperature  $T_{i,cold}/T_e \lesssim 0.4$ , and when there is a significant parallel drift  
 219 between the cold ions and electrons. These features are all consistent with the ion acous-  
 220 tic instability which, in the simple model of a two component plasma, requires  $T_i \ll T_e$   
 221 to avoid Landau damping, and energy for wavegrowth is provided by the drifting elec-  
 222 trons (Baumjohann & Treumann, 1996).

223 Here we limited ourselves to waves found in the magnetospheric separatrix region,  
 224 excluding waves such as those in Fig. 1, found close to the ion edge in the outflow. This  
 225 is because the inclusion of magnetosheath ions often makes it difficult to isolate the cold  
 226 ion component (Li et al., 2017). However, we want to make it clear that the waves are

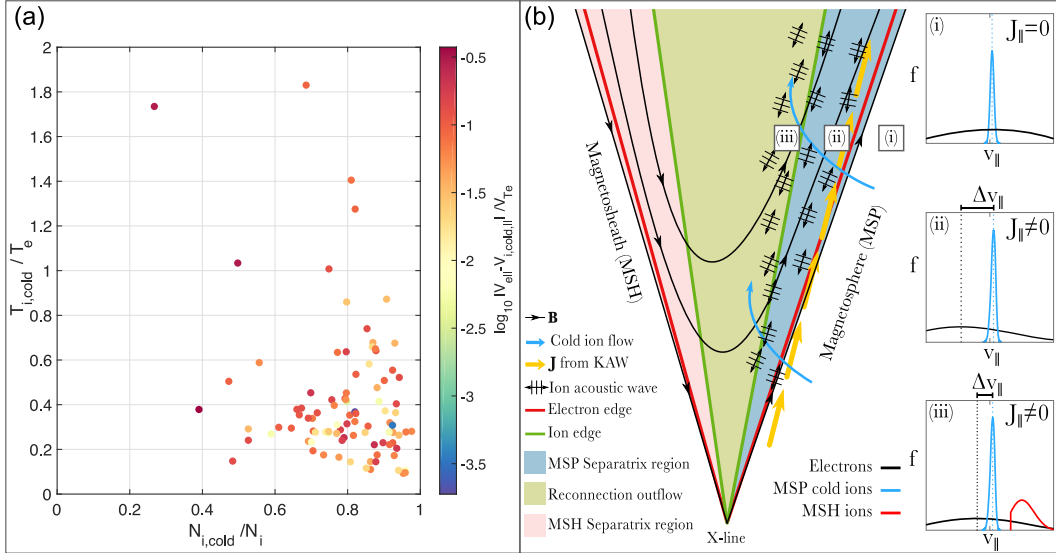


**Figure 4.** (a) Cold plasma properties for waves observed in the magnetospheric separatrix region. (b) Illustration showing where in the reconnection picture the ion acoustic waves are observed and the process leading to their formation. The boxes (i), (ii), and (iii) show where the distribution functions in the right column are observed. The separatrices are the outermost drawn field lines.

227 also often found in the parts of the outflow where cold magnetospheric ions are still the  
 228 dominant ion component, that is, close to the magnetospheric ion edge.

#### 229 4 Discussion

230 With this Letter we aimed at answering two main questions regarding the large am-  
 231 plitude electrostatic waves with frequencies near  $f_{pi}$  which MMS often observes at the  
 232 reconnecting magnetopause. What is their generation mechanism? How do they affect  
 233 the plasma?

234 Regarding the generation mechanism, there are three main pieces of evidence that,  
 235 when combined, strongly points to the ion acoustic instability as the culprit. The first  
 236 piece is the fact that the waves seem to be strongly connected to the ion scales, having  
 237 frequencies around  $f_{pi}$ , and phase speeds in the ion range rather than electron range. This  
 238 suggests that an electron-electron instability is unlikely to be the source, and that ions  
 239 are important. The second piece is the fact that 91% of the waves are found when cold  
 240 ions are dominating and have temperatures well below the electron temperature, giving

241 a strong indication that the cold plasma component is essential. The third piece is the  
 242 fact that for the example event in Fig. 2, Eq. (1) predicts a growing ion acoustic wave.  
 243 It is important to note that due to the dynamic nature of the separatrix region, the elec-  
 244 tron flow is highly variable (as seen by the currents in Fig. 1f), and waves that are grow-  
 245 ing in one instance of time may be stable or even damped in the next, also consistent  
 246 with the localized, patchy, waveforms observed. This is reflected in the large variation  
 247 of speeds shown in Fig. 4a. One result of this is that waves are frequently observed in  
 248 plasma where the waves should be either marginally stable or slightly damped accord-  
 249 ing to the numerical dispersion analysis. These electron variations, and the fact that the  
 250 VDFs are not Maxwellian (contrary to the Maxwellianity assumption used in the ana-  
 251 lytical model) but often much more complex, makes a direct comparison between the-  
 252 ory and observation difficult and not conclusive. However, these observations combined  
 253 lets us conclude that the ion acoustic instability is very likely the source of these waves.

254 To answer the second question, regarding the effect of the waves, we need to take  
 255 a step back and put the information into the context of magnetic reconnection. For the  
 256 ion acoustic instability, the source of the free energy is the fast electron flow, which cor-  
 257 responds to the large  $j_{\parallel}$  observed in the separatrix region. The underlying mechanism  
 258 leading to the formation of  $j_{\parallel}$  is the dynamics of a kinetic Alfvén wave (KAW) propa-  
 259 gating away from the x-line (Vaivads et al., 2010; Huang et al., 2018; Dai, 2018). For the  
 260 event in Fig. 1 there is some evidence of KAW-dynamics. Starting roughly from the ion  
 261 edge crossing, there is a clear correlation between  $v_{ix}$  and  $B_x$ , as well as between  $v_{iy}$  and  
 262  $B_y$ . At around 03:55 we see a large increase of  $j_{\parallel}$  which is associated with an 18.5 nT  
 263 increase of  $B_y$  and a 12.5 mV/m decrease of  $E_x$ . The field ratio  $E_x/B_y$  corresponds roughly  
 264 to 1.2 times the Alfvén speed, and the field directions correspond to Poynting flux di-  
 265 rected away from the x-line. These features are consistent with KAWs propagating away  
 266 from the x-line (Shay et al., 2011; Huang et al., 2018). Analysing the  $B_x$  increase at around  
 267 03:50 yields similar conclusions. By reducing  $j_{\parallel}$  the ion acoustic instability thus effec-  
 268 tively damps the KAWs, thereby providing a coupling between Debye and larger scale  
 269 physics.

270 Observations of ion acoustic waves during ongoing magnetic reconnection has pre-  
 271 viously been reported in a study by Uchino et al. (2017), looking to answer the question  
 272 of which waves are present in the innermost open boundary layer. The authors could not  
 273 directly measure the cold plasma properties due to instrument limitations, and had to

274 instead rely on various assumptions and indirect measurements. Here we confirm with  
 275 directly measured cold plasma properties that the ion acoustic instability can lead to wave  
 276 generation during dayside magnetopause reconnection. Furthermore our statistical re-  
 277 sults show that the ion acoustic instability is likely to be, also in general, responsible for  
 278 the large amplitude, ion plasma frequency waves often observed by MMS in the mag-  
 279 netospheric separatrix region.

280 Finally, we present a schematic picture of the separatrix region (similar to Lindstedt  
 281 et al. (2009)) in Fig. 4b highlighting the kinetic boundaries, to illustrate the generation  
 282 of ion acoustic waves during reconnection when cold ions ( $T_i \ll T_e$ ) are present in the  
 283 magnetosphere. When reconnection is ongoing the cold plasma in the magnetosphere (i)  
 284 is convecting (blue arrows) toward the magnetopause. Here, the lack of free energy pre-  
 285 vents wavegrowth. As the plasma convects further, it passes the KAW propagating in  
 286 the direction of the Alfvén edge out from the ion diffusion region (Vaivads et al., 2010),  
 287 and its associated current (orange arrows) which has a large field-aligned component.  
 288 This  $j_{\parallel}$  corresponds to a  $v_{\parallel}$  shift between electrons and the cold ions as seen in (ii). There  
 289 is thus a positive slope in the electron distribution function, enabling the ion acoustic  
 290 wave to grow via Landau resonance. Throughout the separatrix region we find both par-  
 291 allel and anti-parallel currents as shown in the example of Fig. 1, intermittently enabling  
 292 wavegrowth. Field aligned currents are also present in the outflow region (iii), again re-  
 293 sulting in Landau resonant growth of ion acoustic waves. However, as we move deeper  
 294 into the outflow, the denser and hotter magnetosheath ions starts to dominate, leading  
 295 to Landau damping. This explains why we predominantly see these waves on the mag-  
 296 netospheric side. The end result of this picture is that ion acoustic waves are forming  
 297 throughout the magnetospheric separatrix region, dissipating parallel currents, and damp-  
 298 ing KAWs.

## 299 5 Conclusions

300 We investigate the electrostatic, proton plasma frequency waves with  $E_{\parallel}$  amplitudes  
 301 reaching up to hundreds of mV/m that are frequently found on the magnetospheric side  
 302 of the magnetopause, often in relation to reconnection events. From dispersion analy-  
 303 sis we conclude that the waves are due to an ion acoustic instability between the elec-  
 304 trons and cold magnetospheric ions in the separatrix region. We support this conclusion  
 305 statistically by analyzing waves from 5 months of MMS data, finding 91% of the waves

306 to be observed when cold ions are present. Cold ions, typically with thermal energies in  
307 the range 10-100 eV dominate the density  $n_{i,\text{cold}}/n_i > 0.6$ , and have temperatures lower  
308 than the electrons, typically below  $0.4 T_e$ . This temperature ratio is favourable for ion  
309 acoustic waves. Energy for wavegrowth is provided by significant parallel currents.

310 We conclude that these waves are ion acoustic waves formed when cold magneto-  
311 spheric ions are convected into the separatrix region, where parallel currents drive the  
312 plasma unstable an ion acoustic instability. These ion acoustic waves can be important  
313 for separatrix dynamics on both small and large scales. On small scale the waves are ca-  
314 pable of trapping cold ions, possibly leading to heating, and on a larger scale they are  
315 dissipating parallel currents associated with kinetic Alfvén waves propagating away from  
316 the ion diffusion region.

### 317 **Acknowledgments**

318 We thank the entire MMS team and instrument PIs for data access and support. MMS  
319 data are available at <https://lasp.colorado.edu/mms/sdc/public>. This work is supported  
320 by the Swedish National Space Board, grant 128/17, and the Swedish Research Coun-  
321 cil, grant 2016-05507.

### 322 **References**

- 323 André, M., & Cully, C. M. (2012). Low-energy ions: A previously hidden solar sys-  
324 tem particle population. *Geophysical Research Letters*, *39*(3). doi: 10.1029/  
325 2011GL050242
- 326 Angelopoulos, V. (2008). The THEMIS mission. *Space Science Reviews*, *141*, 5–34.  
327 doi: 10.1007/s11214-008-9336-1
- 328 Baumjohann, W., & Treumann, R. A. (1996). *Basic space plasma physics*. Imperial  
329 College Press.
- 330 Birn, J., & Priest, E. R. (2007). *Reconnection of magnetic fields: magnetohydrody-*  
331 *namics and collisionless theory and observations*. Cambridge University Press.
- 332 Burch, J. L., Moore, T. E., Torbert, R. B., & Giles, B. L. (2016, March). Magne-  
333 topheric Multiscale overview and science objectives. *Space Science Reviews*,  
334 *199*(1), 5–21. doi: 10.1007/s11214-015-0164-9
- 335 Cowley, S. W. H. (2013). Theoretical perspectives of the magnetopause: A tuto-  
336 rial review. In *Physics of the magnetopause* (p. 29-43). American Geophysical

- 337 Union (AGU). doi: 10.1029/GM090p0029
- 338 Dai, L. (2018). Structures of hall fields in asymmetric magnetic reconnection. *Jour-*  
339 *nal of Geophysical Research: Space Physics*, *123*(9), 7332-7341. doi: 10.1029/  
340 2018JA025251
- 341 Dai, L., Wang, C., Zhang, Y., Lavraud, B., Burch, J., Pollock, C., & Torbert,  
342 R. B. (2017). Kinetic Alfvén wave explanation of the hall fields in mag-  
343 netic reconnection. *Geophysical Research Letters*, *44*(2), 634-640. doi:  
344 10.1002/2016GL071044
- 345 Ergun, R. E., Holmes, J. C., Goodrich, K. A., Wilder, F. D., Stawarz, J. E., Eriks-  
346 son, S., ... André, M. (2016). Magnetospheric Multiscale observations of  
347 large-amplitude, parallel, electrostatic waves associated with magnetic recon-  
348 nection at the magnetopause. *Geophysical Research Letters*, *43*(11), 5626-5634.  
349 doi: 10.1002/2016GL068992
- 350 Ergun, R. E., Tucker, S., Westfall, J., Goodrich, K. A., Malaspina, D. M., Summers,  
351 D., ... Cully, C. M. (2016, March). The Axial Double Probe and Fields signal  
352 processing for the MMS mission. *Space Science Reviews*, *199*(1-4), 167-188.  
353 doi: 10.1007/s11214-014-0115-x
- 354 Fairfield, D. H. (1976). Waves in the vicinity of the magnetopause. In B. M. Mc-  
355 Cormac (Ed.), *Magnetospheric particles and fields* (pp. 67-77). Dordrecht:  
356 Springer Netherlands.
- 357 Farrell, W. M., Desch, M. D., Kaiser, M. L., & Goetz, K. (2002). The dominance of  
358 electron plasma waves near a reconnection x-line region. *Geophysical Research*  
359 *Letters*, *29*(19), 8-1-8-4. doi: 10.1029/2002GL014662
- 360 Fried, B. D., & Conte, S. D. (1961). *The plasma dispersion function*. Academic  
361 Press, New York.
- 362 Gosling, J. T., Thomsen, M. F., Bame, S. J., Onsager, T. G., & Russell, C. T.  
363 (1990). The electron edge of low latitude boundary layer during acceler-  
364 ated flow events. *Geophysical Research Letters*, *17*(11), 1833-1836. doi:  
365 10.1029/GL017i011p01833
- 366 Graham, D. B., Khotyaintsev, Y. V., Vaivads, A., & André, M. (2015). Electrostatic  
367 solitary waves with distinct speeds associated with asymmetric reconnection.  
368 *Geophysical Research Letters*, *42*(2), 215-224. doi: 10.1002/2014GL062538
- 369 Graham, D. B., Khotyaintsev, Y. V., Vaivads, A., & André, M. (2016). Elec-

- 370 trostatic solitary waves and electrostatic waves at the magnetopause.  
 371 *Journal of Geophysical Research: Space Physics*, 121(4), 3069-3092. doi:  
 372 10.1002/2015JA021527
- 373 Graham, D. B., Vaivads, A., Khotyaintsev, Y. V., & André, M. (2016). Whistler  
 374 emission in the separatrix regions of asymmetric magnetic reconnection. *Jour-*  
 375 *nal of Geophysical Research: Space Physics*, 121(3), 1934-1954. doi: 10.1002/  
 376 2015JA021239
- 377 Gurnett, D. A., Anderson, R. R., Tsurutani, B. T., Smith, E. J., Paschmann, G.,  
 378 Haerendel, G., ... Russell, C. T. (1979). Plasma wave turbulence at the mag-  
 379 netopause: Observations from isee 1 and 2. *Journal of Geophysical Research:*  
 380 *Space Physics*, 84(A12), 7043-7058. doi: 10.1029/JA084iA12p07043
- 381 Huang, H., Yu, Y., Dai, L., & Wang, T. (2018). Kinetic Alfvén waves excited in two-  
 382 dimensional magnetic reconnection. *Journal of Geophysical Research: Space*  
 383 *Physics*, 123(8), 6655-6669. doi: 10.1029/2017JA025071
- 384 Khotyaintsev, Y. V., Graham, D. B., Norgren, C., & Vaivads, A. (2019). Collision-  
 385 less magnetic reconnection and waves: Progress review. *Frontiers in Astron-*  
 386 *omy and Space Sciences*, 6, 70. doi: 10.3389/fspas.2019.00070
- 387 Khotyaintsev, Y. V., Vaivads, A., Retinò, A., André, M., Owen, C. J., & Nilsson, H.  
 388 (2006, Nov). Formation of inner structure of a reconnection separatrix region.  
 389 *Phys. Rev. Lett.*, 97, 205003. Retrieved from [https://link.aps.org/doi/](https://link.aps.org/doi/10.1103/PhysRevLett.97.205003)  
 390 [10.1103/PhysRevLett.97.205003](https://link.aps.org/doi/10.1103/PhysRevLett.97.205003) doi: 10.1103/PhysRevLett.97.205003
- 391 LaBelle, J., Treumann, R. A., Haerendel, G., Bauer, O. H., Paschmann, G.,  
 392 Baumjohann, W., ... Holzworth, R. H. (1987). AMPTE IRM observa-  
 393 tions of waves associated with flux transfer events in the magnetosphere.  
 394 *Journal of Geophysical Research: Space Physics*, 92(A6), 5827-5843. doi:  
 395 10.1029/JA092iA06p05827
- 396 Lee, J. H., & Angelopoulos, V. (2014). On the presence and properties of cold ions  
 397 near earth's equatorial magnetosphere. *Journal of Geophysical Research: Space*  
 398 *Physics*, 119(3), 1749-1770. doi: 10.1002/2013JA019305
- 399 Li, W. Y., André, M., Khotyaintsev, Y. V., Vaivads, A., Fuselier, S. A., Graham,  
 400 D. B., ... Burch, J. (2017). Cold ionospheric ions in the magnetic reconnect-  
 401 ion outflow region. *Journal of Geophysical Research: Space Physics*, 122(10),  
 402 10,194-10,202. doi: 10.1002/2017JA024287

- 403 Lindqvist, P.-A., Olsson, G., Torbert, R. B., King, B., Granoff, M., Rau, D., ...  
 404 Tucker, S. (2016, March). The Spin-Plane Double Probe electric field  
 405 instrument for MMS. *Space Science Reviews*, 199(1-4), 137–165. doi:  
 406 10.1007/s11214-014-0116-9
- 407 Lindstedt, T., Khotyaintsev, Y. V., Vaivads, A., André, M., Fear, R. C., Lavraud,  
 408 B., ... Owen, C. J. (2009). Separatrix regions of magnetic reconnection  
 409 at the magnetopause. *Annales Geophysicae*, 27(10), 4039–4056. doi:  
 410 10.5194/angeo-27-4039-2009
- 411 Pollock, C., Moore, T., Jacques, A., Burch, J., Gliese, U., Saito, Y., ... Zeuch, M.  
 412 (2016, March). Fast Plasma Investigation for Magnetospheric Multiscale. *Space*  
 413 *Science Reviews*, 199(1-4), 331–406. doi: 10.1007/s11214-016-0245-4
- 414 Russell, C. T., Anderson, B. J., Baumjohann, W., Bromund, K. R., Dearborn,  
 415 D., Fischer, D., ... Richter, I. (2016, March). The Magnetospheric Mul-  
 416 tiscale Magnetometers. *Space Science Reviews*, 199(1-4), 189–256. doi:  
 417 10.1007/s11214-014-0057-3
- 418 Shay, M. A., Drake, J. F., Eastwood, J. P., & Phan, T. D. (2011, Aug). Super-  
 419 alfvénic propagation of substorm reconnection signatures and poynting flux.  
 420 *Phys. Rev. Lett.*, 107, 065001. Retrieved from [https://link.aps.org/doi/](https://link.aps.org/doi/10.1103/PhysRevLett.107.065001)  
 421 [10.1103/PhysRevLett.107.065001](https://link.aps.org/doi/10.1103/PhysRevLett.107.065001) doi: 10.1103/PhysRevLett.107.065001
- 422 Tang, B.-B., Li, W. Y., Graham, D. B., Rager, A. C., Wang, C., Khotyaintsev,  
 423 Y. V., ... Burch, J. L. (2019). Crescent-shaped electron distributions at  
 424 the nonreconnecting magnetopause: Magnetospheric multiscale observations.  
 425 *Geophysical Research Letters*, 46(6), 3024-3032. doi: 10.1029/2019GL082231
- 426 Toledo-Redondo, S., André, M., Khotyaintsev, Y. V., Lavraud, B., Vaivads, A.,  
 427 Graham, D. B., ... Burch, J. L. (2017). Energy budget and mechanisms of  
 428 cold ion heating in asymmetric magnetic reconnection. *Journal of Geophysical*  
 429 *Research: Space Physics*, 122(9), 9396-9413. doi: 10.1002/2017JA024553
- 430 Uchino, H., Kurita, S., Harada, Y., Machida, S., & Angelopoulos, V. (2017). Waves  
 431 in the innermost open boundary layer formed by dayside magnetopause recon-  
 432 nection. *Journal of Geophysical Research: Space Physics*, 122(3), 3291-3307.  
 433 doi: 10.1002/2016JA023300
- 434 Vaivads, A., Khotyaintsev, Y., André, M., Retinò, A., Buchert, S. C., Rogers, B. N.,  
 435 ... Phan, T. D. (2004, Aug). Structure of the magnetic reconnection diffusion

- 436 region from four-spacecraft observations. *Phys. Rev. Lett.*, *93*, 105001. doi:  
437 10.1103/PhysRevLett.93.105001
- 438 Vaivads, A., Retinò, A., Khotyaintsev, Y. V., & André, M. (2010). The Alfvén edge  
439 in asymmetric reconnection. *Annales Geophysicae*, *28*(6), 1327–1331. doi: 10  
440 .5194/angeo-28-1327-2010
- 441 Wilder, F. D., Ergun, R. E., Goodrich, K. A., Goldman, M. V., Newman, D. L.,  
442 Malaspina, D. M., ... Holmes, J. C. (2016). Observations of whistler mode  
443 waves with nonlinear parallel electric fields near the dayside magnetic recon-  
444 nection separatrix by the magnetospheric multiscale mission. *Geophysical  
445 Research Letters*, *43*(12), 5909-5917. doi: 10.1002/2016GL069473
- 446 Wilder, F. D., Ergun, R. E., Hoilijoki, S., Webster, J., Argall, M. R., Ahmadi, N.,  
447 ... Giles, B. L. (2019). A survey of plasma waves appearing near dayside mag-  
448 netopause electron diffusion region events. *Journal of Geophysical Research:  
449 Space Physics*, *124*(10), 7837-7849. doi: 10.1029/2019JA027060
- 450 Zhou, M., Ashour-Abdalla, M., Berchem, J., Walker, R. J., Liang, H., El-Alaoui, M.,  
451 ... Chandler, M. O. (2016). Observation of high-frequency electrostatic waves  
452 in the vicinity of the reconnection ion diffusion region by the spacecraft of the  
453 Magnetospheric Multiscale (MMS) mission. *Geophysical Research Letters*,  
454 *43*(10), 4808-4815. doi: 10.1002/2016GL069010